Raman Spectra of Graphite Oxide and Functionalized Graphene Sheets

Konstantin N. Kudin,[†] Bulent Ozbas,[‡] Hannes C. Schniepp,[‡] Robert K. Prud'homme,[‡] Ilhan A. Aksay,[‡] and Roberto Car*,[†]

Department of Chemistry, and Department of Chemical Engineering, Princeton University, Princeton, New Jersey 08544

Received July 26, 2007; Revised Manuscript Received October 25, 2007

ABSTRACT

We investigate Raman spectra of graphite oxide and functionalized graphene sheets with epoxy and hydroxyl groups and Stone–Wales and 5–8–5 defects by first-principles calculations to interpret our experimental results. Only the alternating pattern of single–double carbon bonds within the sp^2 carbon ribbons provides a satisfactory explanation for the experimentally observed blue shift of the G band of the Raman spectra relative to graphite. To obtain these single–double bonds, it is necessary to have sp^3 carbons on the edges of a zigzag carbon ribbon.

Motivated by the promise of graphene as an alternative to single-wall carbon nanotubes, in recent studies, we reported[1,2] a method to produce functionalized single graphene sheets (FGSs) in bulk quantities through thermal expansion of graphite oxide (GO). The aromaticity of the graphene sheets is lost as epoxide and hydroxyl groups are also formed during the oxidation process, resulting in an interlayer spacing (*d*-spacing) increase from 0.34 to ~0.7 nm.[1] Pressure buildup due to CO_2 release during rapid heating separates stacked GO layers to produce functionalized single graphene sheets. While the C/O ratio of GO is ~2, the FGS produced by this approach has a C/O ratio of 10−20 as some of the epoxide and hydroxyl sites are eliminated.[2]

Both from a practical and a fundamental perspective, it is important to understand the nature of disorder in GO and FGSs. Despite the fact that GO has been known since 1859 and several GO models[3−7] have been suggested, its detailed structure is still under debate, and a definitive atomistic model is not yet available. For a detailed understanding of mechanical and electronic properties of the FGS, we would like to know (i) if the honeycomb carbon network of graphene remains essentially intact or if rings other than six-membered rings and other topological defects appear in the oxidation process; (ii) if the epoxy and hydroxyl groups are distributed randomly, if they retain some amount of short/intermediate range order, or if they tend to cluster, creating patches of more strongly oxidized graphene intermixed with patches of near-perfect graphene; and (iii) if a portion of the defect anneals during the thermal treatment process.

To provide answers to some of these questions, here, we report our work on the characterization of GO and FGSs by Raman spectroscopy and scanning tunneling microscopy (STM). We also report calculated vibrational spectra of various functional fragments that might appear during the chemical transformation of graphite to determine which spectroscopic features appear for a particular atomic arrangement. Specifically, using plane wave density functional theory (DFT)[8] calculations, we have computed the Raman spectra of graphene sheets with defects, as well as epoxy and hydroxyl groups attached in various configurations. The presence of such groups in GO was deduced from NMR spectroscopy and group-specific reaction chemistry by Lerf et al.[7] In the processing of similar materials—carbon nanotubes—oxidation also plays an important role when purifying nanotubes in order to remove the amorphous carbon.[9]

Raman spectroscopy is a widely used tool for the characterization of carbon products, especially considering the fact that conjugated and double carbon−carbon bonds lead to high Raman intensities. However, we are aware of only one previous computational study that investigated the Raman spectra of oxidized nanotubes modeled by relatively short nanotube segments terminated with hydrogen.[10] This geometry introduced spurious features into the vibrational modes, making the interpretation of the experimental spectroscopic features somewhat challenging. Another work[11] calculated the infrared spectra of various finite graphitic structures with edge groups. Since most GO models involve a mostly intact hexagonal carbon lattice, placing chemical groups randomly throughout the 2D sheet and not on the edges should model the GO structure more accurately.

Highly ordered graphite has only a couple of Raman-active bands visible in the spectra (Figure 1), the in-phase vibration

---

* To whom correspondence should be addressed. E-mail: rcar@princeton.edu.
† Department of Chemistry, Princeton University.
‡ Department of Chemical Engineering, Princeton University.
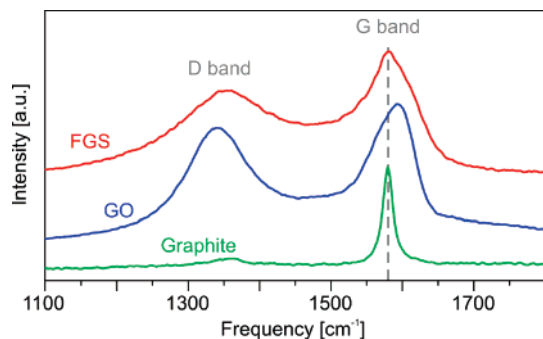
Figure 1. Evolution of the Raman spectra during the oxidation and exfoliation processes for graphite, GO, and FGS. All of the spectra correspond to an exciting laser wavelength of 514.5 nm. The position of the G band peak in graphite is indicated by a vertical, dashed line.

Table 1: Raman Peak Positions and Left and Right Widths at Half-Maximum

| material	LWHM [cm^{-1}]	peak [cm^{-1}]	RWHM [cm^{-1}]
graphite	9	1580	8
GO	55	1593	28
FGS	55	1581	43

of the graphite lattice (G band) at 1575 cm^{-1} as well as the (weak) disorder band caused by the graphite edges (D band) at approximately 1355 cm^{-1}.[12] (Raman spectra of samples were measured using a Renishaw 1000 microspectrometer using an excitation wavelength of 514.5 nm. All samples were deposited on silicon wafers in powder form without using any solvent. The fluorescence background for the GO spectra was subtracted using the Wire 2.0 Renishaw software.) While the lattice vibration with the frequency of the D band is, in fact, present in the infinite graphene sheet, it remains Raman-inactive until the edges "light" it up due to the symmetry breaking and the corresponding change in the selection rules. Both the G and the D bands undergo significant changes upon amorphization of graphite as amorphous carbon contains a certain fraction of sp^3 carbons.[13] A universal observation is that higher disorder in graphite leads to a broader G band, as well as to a broad D band of higher relative intensity compared to that of the G band.

GO to FGS transformation leaves behind topological defects and vacancies.[1,2] Among the vacancies, one of the more stable ones is the double vacancy (C$_2$), which is composed of two pentagonal rings and one octagonal ring and is usually referred to as the 5−8−5 defect.[14] In addition to such 5−8−5 defects, we have also investigated the common 5−7−7−5 rings, that is, the so-called Stone−Wales (SW) defects, which play an important role in carbon nanotubes and other graphitic materials.[15] Along the graphite−GO−FGS path, the Raman spectra undergo changes (Figure 1) that are similar to those observed in the graphite to amorphous carbon transition.[13] Specifically, the G band broadens significantly and displays a shift to higher frequencies (blue-shift), and the D band grows in intensity. Table 1 indicates the peak positions of the G band in the materials we have investigated, as well as the corresponding left and

right widths at half-maximum (LWHM and RWHM, respectively), which were calculated with respect to a baseline obtained by drawing a tangent line to the spectrum between 800 and 2,200 cm^{-1}. A notable fact is that while the G band peak is located at a higher frequency in GO than that in graphite (1593 vs 1580 cm^{-1}), in FGS, it is located almost at the same frequency as that in graphite. We stress that in all measurements, we have consistently used the same laser excitation frequency (514.5 nm). Thus, we can exclude spurious shifts due to changes in the laser frequency, which are known to affect the D band of graphite.[16]

As in the case of our Raman spectra of GO, the G band initially shifts to higher frequencies during graphite amorphization.[13] A literature survey points to several possible explanations for this blue shift. First, in graphite with a sufficient concentration of defects, there is another band, the D′ band, located at 1620 cm^{-1},[12,17−19] which can partially merge with the G band. The explanation given for the appearance of this band is that in graphite, there is a nonzero phonon density of states above the G band; such phonons, which are usually Raman-inactive, become active due to phonon confinement caused by the defects.[19] Second, when going from a graphite crystal to a single graphene sheet, the G band shifts from 1581 to 1585 cm^{-1}; this shift could also be partially responsible for the higher G band frequencies in GO if significant unmodified graphitic areas remain.[20] Finally, isolated double bonds resonate at higher frequencies than the G band of graphite,[13] although the specific patterns of the double bonds causing such an upshift, to the best of our knowledge, are not known. Compared to the G band of graphite, the blue-shifted peaks due to the first two causes are usually relatively weak. Therefore, the third alternative, namely, the presence of double bonds, appears to be the most plausible explanation of the blue shift of the G band that we observed experimentally; we revisit this issue in great detail later in the paper.

In FGSs, the G band shifts back to the position (Figure 1) of the G band in graphite, which we attribute to a graphitic "self-healing" similar to what was observed from the sharpening of the G peak and the intensity decrease of the D peak in heat-treated graphite.[21,22] In fact, in our STM experiments, we do observe the re-emergence of graphitic order in FGSs, as can be seen in Figure 2. (An amount of 5 mg of FGS was mixed with 5 mL of dimethylformamide (DMF) and ultrasonicated for 30 min. The obtained dispersion was spin-cast onto a freshly cleaved sheet of highly oriented pyrolytic graphite (HOPG) at 5000 rpm. The sample was investigated by scanning tunneling microscopy (STM; Veeco MultiMode/NanoScope IIIa, Veeco Metrology LLC, Santa Barbara, CA, U.S.A.) using cut Pt/Ir tips at ambient conditions.) Compared to a STM image of highly oriented pyrolytic graphite (HOPG) taken under identical conditions (inset at the left bottom), FGS appears rough, featuring a peak-to-peak topography of 1 nm. This roughness—due to functional groups and defects[1]—prevents us from obtaining atomic resolution in all areas of the sheet. Nevertheless, the absolute value of the Fourier transform of the image (inset at the right top; hexagonal symmetry highlighted by manually
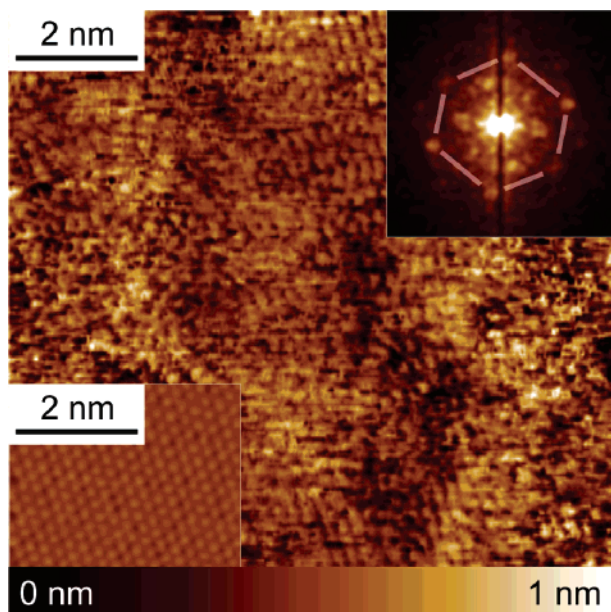
Figure 2. A 10×10 nm STM topography image of a FGS, taken at a bias voltage of 30 mV and a current of 5 nA. To minimize possible artifacts due to the size of the probe, the image was taken on top of a wrinkle of the sheet, where the topography is convex. The Fourier transform of the image shows that the hexagonal order is present (inset on the right top). The inset on the left bottom shows a STM image of HOPG taken under identical conditions (same topography color map as the main image).

added lines) shows a clear signature of a graphitic backbone. This indicates that the sheets undergo annealing during the reduction process. A recently proposed atomistic mechanism of graphite defect annealing can very well be responsible for such a behavior.[23,24]

The Raman spectra calculations were performed with the Quantum-Espresso (QE) package.[25] Theoretical evaluation of the Raman spectra requires first-, second-, and third-order energy derivatives, among which the most demanding are the second-order derivatives of the energy with respect to the atomic positions (force constants)[26] and the third-order polarizability derivatives, twice with respect to the electric field (yielding polarizability) and once with respect to the atomic positions (Raman intensity tensors). The important advantage of the QE code is that the polarizability derivatives have been recently implemented via a second-order response formalism,[27] thus making their calculation relatively inexpensive compared to that of the force constants. To avoid the effect of the finite edges, we adopt a periodic supercell approach, using a 4×4 hexagonal supercell containing 16 graphene unit cells with 2 atoms each. In the third direction, we use a large enough spacing (1.23 nm) to make periodic image effects negligible. The resulting 32 carbon atom supercell is sufficient to investigate the $5-8-5$ and $5-7-7-5$ defects with reasonable isolation, as well as a variety of low-coverage oxidation products. In all of our calculations, we used the Becke−Lee−Yang−Parr (BLYP) exchange−correlation functional[28] and treated the valence−core interaction for the electrons with norm-conserving pseudopotentials.[29] We simultaneously optimized the two lattice vectors in the plane and the atomic positions in the supercell by variable cell dynamics.[30] The residual stress in the optimized structures did not exceed 300 MPa. In some cases, such as with highly nonplanar geometries or with $5-8-5$ and $5-7-7-5$ topological defects, there were significant changes ($\sim5\%$) in the lattice vector lengths as a result of the optimization. To avoid asymmetric stresses, we placed the functional groups in pairs on the opposite sides of the sheet, with significant isolation from each other whenever possible. In this way, any buckling was symmetrically compensated. We used a plane wave expansion cutoff of 80 Ry for the wave functions and of 320 Ry for the charge density in the fixed cell calculations, while higher cutoffs were employed in the variable cell calculations (95 and 380 Ry, respectively, using the modified kinetic energy functional introduced in ref 31). The Gamma point was used for the k-space integration. Notice that the Gamma point of the 4×4 graphitic supercell unfolds in the graphene unit cell into a k-mesh that excludes the K point at the Brillouin zone boundary, where the valence and conduction bands of graphene are degenerate. This point would yield an infinite perturbative response in a calculation for an ideal graphene sheet. The Raman G peak for our 32 atom graphene supercell optimized with variable cell dynamics occurs at 1586 cm^{-1}, in excellent agreement with the experimental value of 1585 cm^{-1} in single graphene sheets.[20] In the following, we report atomic structure pictures, which were drawn with the help of the GaussView program.[32] The Raman spectra corresponding to the various structures were broadened by convoluting the calculated Raman lines with a Gaussian having a fwhm of 12 cm^{-1}.

First, following the GO model of Lerf et al.,[7] we calculated the Raman spectra of graphene with added oxygen-containing groups, both with the epoxy groups isolated (OX1 in Figure 3a) and arranged in a pair at the opposite edges of the same six-membered ring (OX2 in Figure 3b). The latter structure was found to be a precursor for lattice unzipping[33] in a previous study by our group. We also investigated the structures obtained by hydrolyzing the isolated epoxy groups, with two hydroxyls per pre-existing epoxy group. Here, we considered a pair of hydroxyl groups in the 1,2-position (ortho attachment in benzene) on the opposite sides of the sheet (OH1 in Figure 3c). In addition, we also investigated two nearby pairs of hydroxyl groups in the 1,4-positions (para attachment in benzene) such that an isolated double bond is formed (OH2 in Figure 3d, in which the atoms participating in the isolated double bond are shown in green).

The first noticeable effect of the addition of epoxy and hydroxyl groups (Figure 4) is a broadening of the graphite G band resulting from a series of new high-intensity bands that are red-shifted with respect to the G band of pure graphite. In contrast, blue-shifted Raman-active bands can only be found in a structure with well-defined double bonds, albeit the intensity of such bands is low. Specifically, only the OH2 structure has such a peak due to the single isolated double bond. Second, the hydroxyl groups yield a series of bands around 1300 cm^{-1}, which is exactly in the same range where the broad D band is located in the experimental data. Overall, due to the closeness in the frequencies of the sp^3
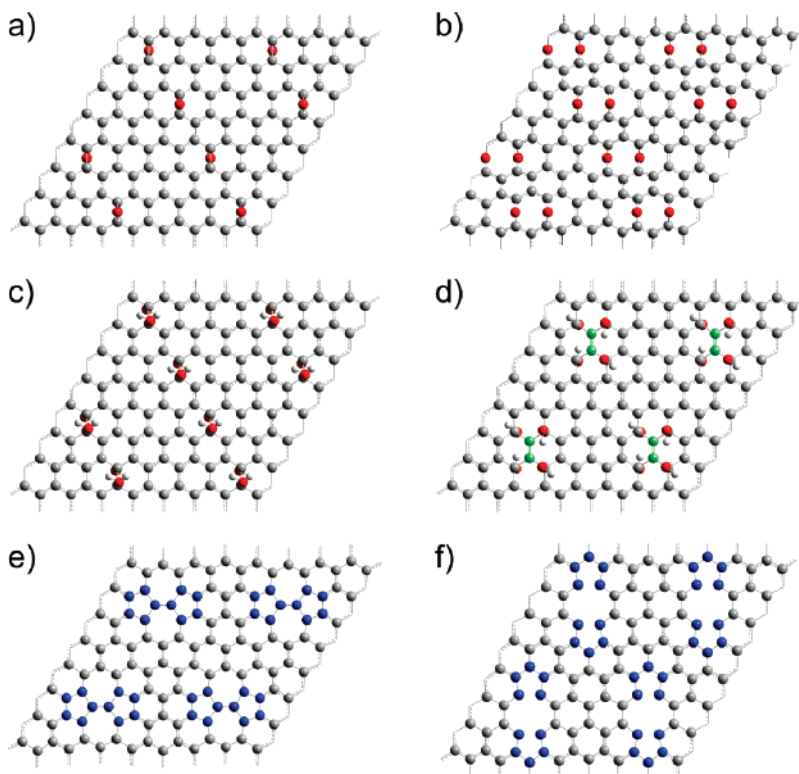
Figure 3. The 2 × 2 replicated cells with various groups and defects. Note that single, double, and conjugated bonds are drawn according to the distance criteria by GaussView.[32] (a) Graphene with individual epoxy groups (OX1). (b) Graphene with two epoxy groups arranged in a pre-unzipping pattern (OX2). (c) Graphene after hydrolysis, with a 1,2-hydroxyl pair per epoxy group (OH1). (d) Graphene with two 1,4-hydroxyl pairs (OH2), forming an isolated double bond (contributing atoms colored green). (e) Graphene with the 5−7−7−5 defect (SW). (f) Graphene with a C_2 vacancy (relaxed 5−8−5 defect structure).
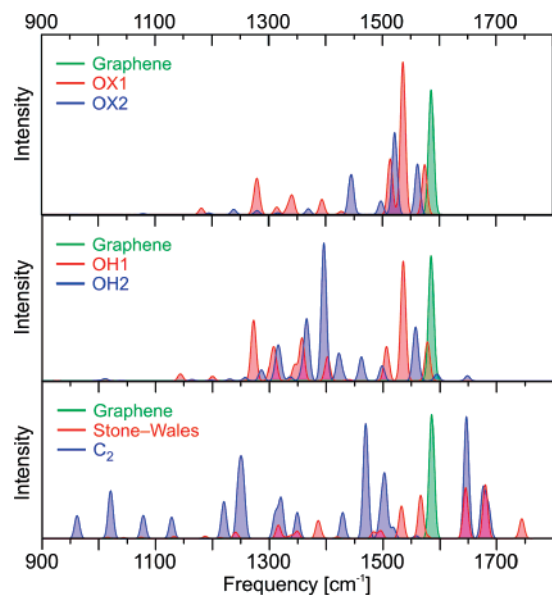

Figure 4. Calculated Raman spectra of graphene, OX1, OX2, OH1, OH2, a C_2 vacancy, and a SW defect.

carbon Raman-active band and the D band of graphite, both types of bands will tend to merge into a broad spectral feature.

The puzzling aspect of the Raman spectra of the model systems that we have considered so far is that none of the isolated and semi-isolated epoxy and hydroxyl groups produce any blue-shifted bands with high Raman intensity.

To obtain a high Raman intensity, a delocalized system of π-electrons is needed, and as we have seen in the example of the OH2 structure, isolated double bonds are insufficient in this respect. The Scholz−Boehm GO model[5] (recently advocated by Szabo et al.[34]) contains sp^2 ribbons with a rigid quinoidal structure (similar to R1 in Figure 5a). Since these ribbons are the narrowest possible, the double bonds are all isolated. However, if ribbons of this type have more than just one layer of sp^2 carbons, they develop a well-defined pattern of alternating single and double bonds within the interconnected sp^2 carbon region, displayed as R2 in Figure 5b. In R2, the calculated Raman-active band is at 1620 cm^{-1}, that is, blue-shifted compared to pure graphite (Figure 5d). Moreover, because of the interconnected sp^2 carbons, π-electrons are delocalized within the ribbon, and the Raman intensity of the blue-shifted band is high, in contrast to R1. Removal of half of the hydroxyl groups from such a structure results in the structure indicated as R3 in Figure 5c. In R3, we observe that the single−double bond length alternation disappears with a subsequent shift of the G band back to graphitic values. The Scholz−Boehm structure itself, R1, does have a Raman-active band due to isolated double bonds at a relatively high frequency of 1690 cm^{-1}, albeit with a low intensity due to the disappearance of the chains of sp^2 carbon atoms.

Although the R2 structure has the blue-shifted peak observed in the experiment, it also has another peak of high intensity at 1390 cm^{-1} which is not found in the experimental
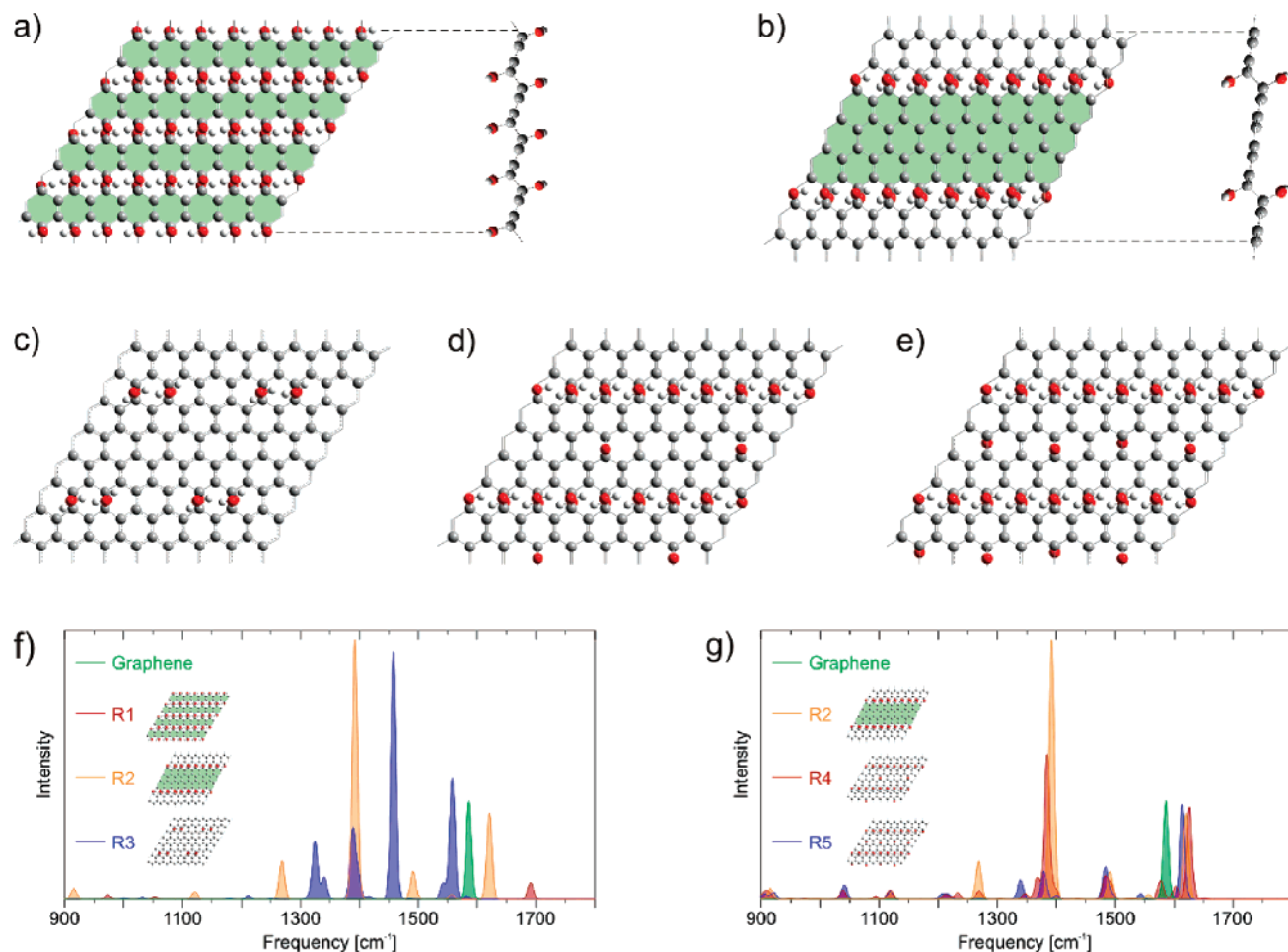
Figure 5. (a) GO with the narrowest ribbons (R1), as per the Scholz−Boehm model (see text), (b) GO with wider ribbons (R2), and (c) GO without ribbons (R3). The hexagons that are part of the ribbons are highlighted in green. (d) R2 structure with an additional epoxy group in the middle of the ribbon (R4). (e) R2 structure with two additional epoxy groups (R5). (f and g) The calculated Raman spectra are shown, with intensities for R1 and R2 multiplied by 10 and 0.5, respectively. Note that in panels a−e the 2 × 2 replicated computational cells are shown, and single, double, and conjugated bonds are drawn according to the distance criteria by GaussView.[32]

data. Furthermore, the R2 structure does not have enough oxygen atoms to match the C/O ratio (2/1) measured for GO. To address both of these concerns, we have investigated the structures R4 and R5 that have additional epoxy groups in the middle of the sp^2 ribbon with respect to R2. Both of these structures can be viewed as intermediates on the path from R2 to R1. By hydrolysis and addition of extra epoxy/hydroxyl groups, R4 and R5 would become R1. Remarkably, in these new structures, we find that the intensity of the peak at 1390 cm^{-1} decreases substantially, while the blue-shifted peak is preserved at roughly the same frequency, thus yielding a much better overall agreement with the experimental spectra in Figure 1.

An important comment is related to the resulting thickness of the carbon sheet due to these types of functionalization. As the side views of the structures in Figure 5 indicate, the ribbons introduce out-of-plane zigzag distortions into the carbon lattice. The heights of these steps are 90, 120, and 100 pm for the structures R1, R2, and R3, respectively. Therefore, in all cases, the effect of the carbon lattice "steps" on the GO profile is negligible, and it is mostly the sidegroups that yield the 0.7 nm thickness in GO.

Finally, we have investigated the Raman spectra of a SW (5−7−7−5) defect (Figure 3e)[15] and a C_2 vacancy (5−8−5) defect (Figure 3f).[14] As noted earlier, in these cases, the supercell does change quite significantly upon relaxation. The C_2 vacancy causes a significant reduction in the lattice vectors, which is not surprising since 2 out of 32 carbon atoms are removed. Although the optimized 5−8−5 defect does not have any local curvature and within the 2D supercell stays completely flat, we found, in preliminary tests, that the defect is more stable on curved surfaces such as, for example, nanotubes. Therefore, if present in sufficient concentrations, these defects might be able to induce curvature in small flakes like those studied in ref 1. Specifically, in small flakes, the curvature would be determined by the balance of the energy gain due to the 5−8−5 defect relaxation and the energy loss due to the strain induced on the nearby graphitic carbons. Overall, the Raman spectra for the C_2 vacancy and the SW defect have a lot of new features, with the notable fact that there is a series of bands above the G band of graphite. Specifically, the C_2 vacancy has Raman peaks at 1647, 1676, and 1686 cm^{-1} (the latter two almost merge in the figure), whereas the SW defect has

peaks at 1645 and 1680 cm^{-1}, as well as at 1744 cm^{-1}. It is worth noting that our calculations yield Raman peaks in the vicinity of 1645 and 1680 cm^{-1} for both structures. Upon examination of the atoms participating in these normal modes, we find that these vibrations derive from the displacements of the carbon atoms which belong simultaneously to five- and six-membered rings, a configuration shared by both structures. Thus, the defects are also capable of producing blue shifts. However, the experimental data do not show significant Raman intensities above 1650 cm^{-1} for both GO and FGS, suggesting that the concentration of such defects in both materials should not be very high. In the case of GO, this is not surprising since a plausible mechanism for the appearance of such defects in large numbers during the oxidation process is not known at the moment. In FGSs, in contrast, the emergence of such defects through carbon emission during reduction is probable.[1] The absence of a Raman signal in the corresponding spectral range, however, suggests that many of these defects may have been removed through annealing. The remaining ones may be concentrated in the few areas where the sheets are wrinkled, as their presence has been associated with curved structures.[1]

In summary, in our experimental work on the transformation from graphite to GO, one of the most puzzling aspects is the blue shift of the graphitic G band in graphite oxide while a reversal is observed after partial reduction to produce FGSs. Computationally, among all of the structures that we have considered, only the alternating pattern of single−double carbon bonds within the sp^2 carbon ribbons as well as the SW and the 5−8−5 defect structures yields Raman bands of high intensity that are blue-shifted compared to the G band of graphite. While isolated double bonds can also lead to blue-shifted bands, the Raman intensity of such bands is significantly lower. To obtain single−double bond alternation within extended sp^2 carbon areas, it is necessary to have sp^3 carbons on the edges of a zigzag carbon ribbon. The Scholz−Boehm GO model introduced the narrowest ribbons of this type; however, in such narrow ribbons the double bonds are all isolated, yielding low blue-shifted Raman intensities in correspondence with the double bonds. The structures that yield the best match with experiment have wider ribbons, as we advocate, with some additional epoxy groups in the middle. The out-of-plane distortions introduced to the carbonaceous backbone by the structures investigated here are around 0.1 nm, implying that the sheets essentially remain flat. One of the most significant findings of this work is that a novel GO model containing areas of sp^2 carbons with an alternating pattern of single−double carbon bonds is able to explain the experimentally observed blue G band shift in GO.

References

(1) Schniepp, H. C.; Li, J.-L.; McAllister, M. J.; Sai, H.; Herrera-Alonso, M.; Adamson, D. H.; Prud'homme, R. K.; Car, R.; Saville, D. A.; Aksay, I. A. *J. Phys. Chem. B* **2006**, *110*, 8535.

(2) McAllister, M. J.; Li, J.-L.; Adamson, D. H.; Schniepp, H. C.; Abdala, A. A.; Liu, J.; Herrera-Alonso, M.; Milius, D. L.; Car, R.; Prud'homme, R. K.; Aksay, I. A. *Chem. Mater.* **2007**, *19*, 4396.

(3) Hofmann, U.; Holst, R. *Ber. Dtsch. Chem. Ges.* **1939**, *72*, 754.

(4) Ruess, G. *Monatsh. Chem.* **1946**, *76*, 381.

(5) Scholz, W.; Boehm, H. P. *Z. Anorg. Allg. Chem.* **1969**, *369*, 327.

(6) Nakajima, T.; Mabuchi, A.; Hagiwara, R. *Carbon* **1988**, *26*, 357.

(7) Lerf, A.; He, H. Y.; Forster, M.; Klinowski, J. *J. Phys. Chem. B* **1998**, *102*, 4477.

(8) Kohn, W.; Sham, L. J. *Phys. Rev.* **1965**, *140*, A1133.

(9) Rinzler, A. G.; Liu, J.; Dai, H.; Nikolaev, P.; Huffman, C. B.; Rodriguez-Macias, F. J.; Boul, P. J.; Lu, A. H.; Heymann, D.; Colbert, D. T.; Lee, R. S.; Fischer, J. E.; Rao, A. M.; Eklund, P. C.; Smalley, R. E. *Appl. Phys. A* **1998**, *67*, 29.

(10) Irle, S.; Mews, A.; Morokuma, K. *J. Phys. Chem. A* **2002**, *106*, 11973.

(11) Fuente, E.; Menendez, J. A.; Diez, M. A.; Suarez, D.; Montes-Moran, M. A. *J. Phys. Chem. B* **2003**, *107*, 6350.

(12) Tuinstra, R.; Koenig, J. L. *J. Chem. Phys.* **1970**, *53*, 1126.

(13) Ferrari, A. C.; Robertson, J. *Phys. Rev. B* **2000**, *61*, 14095.

(14) Lee, G. D.; Wang, C. Z.; Yoon, E.; Hwang, N. M; Kim, D. Y.; Ho, K. M. *Phys. Rev. Lett.* **2005**, *95*, 205501.

(15) Stone, A. J.; Wales, D. J. *Chem. Phys. Lett.* **1986**, *128*, 501.

(16) Kawashima, Y.; Katagiri, G. *Phys. Rev. B* **1995**, *52*, 10053.

(17) Nemanich, R. J.; Solin, S. A. *Phys. Rev. B* **1979**, *20*, 392.

(18) Livneh, T.; Haslett, T. L.; Moskovits, M. *Phys. Rev. B* **2002**, *66*, 195110.

(19) Cancado, L. G.; Pimenta, M. A.; Neves, B. R. A.; Dantas, M. S. S.; Jorio, A. *Phys. Rev. Lett.* **2004**, *93*, 247401.

(20) Graf, D.; Molitor, F.; Ensslin, K.; Stampfer, C.; Jungen, A.; Hierold, C.; Wirtz, L. *Nano Lett.* **2007**, *7*, 238.

(21) Han, C. C.; Lee, J. T.; Chang, H. *Chem. Mater.* **2001**, *13*, 4180.

(22) Sato, K.; Saito, R.; Oyama, Y.; Jiang, J.; Cancado, L. G.; Pimenta, M. A.; Jorio, A.; Samsonidze, G. G.; Dresselhaus, G.; Dresselhaus, M. S. *Chem. Phys. Lett.* **2006**, *427*, 117.

(23) Ding, F.; Jiao, K.; Wu, M. Q.; Yakobson, B. I. *Phys. Rev. Lett.* **2007**, *98*, 075503.

(24) Ding, F.; Jiao, K.; Lin, Y.; Yakobson, B. I. *Nano Lett.* **2007**, *7*, 681.

(25) Quantum Espresso. http://www.quantum-espresso.org.

(26) Baroni, S.; de Gironcoli, S.; Dal Corso, A.; Giannozzi, P. *Rev. Mod. Phys.* **2001**, *73*, 515.

(27) Lazzeri, M.; Mauri, F. *Phys. Rev. Lett.* **2003**, *90*, 036401.

(28) (a) Becke, A. D. *Phys. Rev. A* **1988**, *38*, 3098. (b) Lee, C. T.; Yang, W. T.; Parr, R. G. *Phys. Rev. B* **1988**, *37* , 785.

(29) Hamann, D. R.; Schluter, M.; Chiang, C. *Phys. Rev. Lett.* **1979**, *43*, 1494.

(30) Wentzcovitch, R. M.; Martins, J. L.; Price, G. D. *Phys. Rev. Lett.* **1993**, *70*, 3947.

(31) Bernasconi, M.; Chiarotti, G. L.; Focher, P.; Scandolo, S.; Tosatti, E.; Parrinello, M. *J. Phys. Chem. Solids* **1995**, *56*, 501.

(32) Dennington, R., II; Keith, T.; Millam, J.; Eppinnett, K.; Hovell, W. L.; Gilliland, R. *GaussView*, version 3.09; Semichem, Inc.: Shawnee Mission, KS, 2003.

(33) Li, J.-L.; Kudin, K. N.; McAllister, M. J.; Prud'homme, R. K.; Aksay, I. A.; Car, R. *Phys. Rev. Lett.* **2006**, *96*, 176101.

(34) Szabo, T.; Berkesi, O.; Forgo, P.; Josepovits, K.; Sanakis, Y.; Petridis, D.; Dekany, I. *Chem. Mater.* **2006**, *18*, 2740.

NL071822Y